Pergamon

Int. J. Heat Mass Transfer. Vol. 39, No. 14, pp. 3003–3019, 1996

0017-9310/96 $15.00 + 0.00

0017-9310(95)00341-X

Stagnation point flow of a chemically reactive fluid in a catalytic porous bed

B. H. CHAO, H. WANG and P. CHENG

Department of Mechanical Engineering, University of Hawaii at Manoa, Honolulu, HI 96822, U.S.A.

(*Received* 27 *December* 1994 *and in final form* 12 *September* 1995)

Abstract—The heat transfer and reaction characteristics of a chemically reactive flow near the stagnation point of a catalytic porous bed with finite thickness are investigated theoretically. Due to the catalytic effect, the activation energy is reduced such that chemical reaction in the bed becomes possible even at relatively low flow temperatures. The steady state and initial transient period in the gas phase upstream and in the catalytic porous bed are studied using both the singular perturbation method and the finite difference method. For the perturbation analysis, a single layer model is sufficient when the bed is relatively thin, of the order of the characteristic thermal diffusion length scale. For a thick bed, a multiple layer analysis is necessary. Results from the steady-state analysis show that for a higher chemical reactivity, lower flow velocity gradient, lower activation energy, and lower mass diffusion rate, the conversion rate from reactants to products is higher so that a thinner bed can be used to reach complete reaction. Moreover, due to the high thermal conductivity of the solid porous material, temperature profiles are modified by the heat release through chemical reaction only slightly for a thin bed. The flow temperature is affected by the reaction more significantly for a thicker bed because more heat is released from the reaction, and the increased importance of convection effect. Numerical results for the transient case exhibit the same characteristics as in the steady state. Copyright © 1996 Elsevier Science Ltd.

1. INTRODUCTION

Chemically reactive flows in porous media have recently received attention because of their practical importance relating to energy utilization and environmental cleanup. Examples are combustion *in situ* in underground reservoirs for enhanced oil recovery [1], ceramic radiant porous burners used by industrial firms as an efficient heat transfer device [2], and the reduction of hazardous combustion products using catalytic porous beds. It is the last application that motivates the present study.

It is well known that exhaust gases from internal combustion engines usually contain carbon monoxide, residual hydrocarbons and nitrogen oxides that are hazardous to living organisms, so their formation must be reduced to an acceptable level. Regulations have been imposed by the government to reduce the negative impact of air quality from automobiles' exhaust gases. A review by McDermott [3] indicated that catalytic converters are the only available technology in the automobile industry to meet the most stringent emission control standards. A catalytic converter is essentially a porous bed which converts the residual hydrocarbons and carbon monoxide to carbon dioxide and water vapor at relatively low temperatures. The physical structure of a catalytic converter shows that the flow in the catalytic bed is a combination of a one-dimensional flow and a stagnation point flow, but more like the latter. To facilitate the investigation, the problem is idealized as a stagnation point flow impinging a catalytic porous bed with a finite thickness.

The problem of gaseous premixed combustion in the stagnation point flow has been analyzed extensively due to its fundamental importance. The propagation of a premixed stagnation point flame has been extensively studied adopting both the constant density [4–6] and variable density [7, 8] approximations. Only quantitative differences were observed between these two approaches. The stagnation point flame against a catalytic surface with the flame attached to the surface has also been studied [9, 10]. In these analyses, the flame temperature, standoff distance, and extinction condition were solved versus the effect of strain rate by adopting a one-step, overall and irreversible reaction following the Arrhenius kinetics with high activation energy.

Transport phenomena in porous media differ from those in the gas phase in two important aspects. Firstly, an additional drag force exists in the flow field due to the existence of solid particles, which is usually much larger than the viscous force and consequently the latter can be neglected in the momentum equation. If the flow velocity is small and the characteristic particle size is much smaller than the hydrodynamic length scale of interest, Darcy's law can be used as the momentum equation [11]. Secondly, the effective stagnant thermal conductivity of a saturated porous medium depends on the thermal conductivities of both the solid and gas phases [12], which is much higher than that of the gas alone because the thermal con-

NOMENCLATURE

a, b	integration constants
B	pre-exponential factor
c_p	specific heat of the gas at constant pressure
c_s	specific heat of the solid porous material
D	mass diffusion coefficient
Da	Damköhler number defined as $B/\rho k$
E	activation energy
$\tilde{E}$	rescaled nondimensional activation energy
F_i, G_i	functions defined after equation (33)
h	reciprocal of the rescaled porous bed thickness
H	thickness of the porous bed
H_{min}	minimum porous bed thickness to reach 99% conversion
k	velocity gradient, also the strain rate, of the flow
K	permeability of the porous bed
Le	Lewis number defined as $\lambda/(\rho D c_p)$
q	heat of combustion per unit mass of the controlling reactant
R	universal gas constant
t	time
t_s	time to reach steady state
T	temperature
u, v	flow velocity along (x, y) directions
x, y	spatial coordinates
Y	mass fraction of the controlling species
z	rescaled nondimensional spatial coordinate defined as $z = \hat{y}/\hat{H}$.

Greek symbols

α	parameter defined after equation (63)
γ, ϕ	parameter defined after equation (53)
Γ, Φ	function defined after equation (53)
ε	small parameter defined as $1/\hat{\lambda}^{1/2}$
φ	porosity of the porous bed
λ	thermal conductivity of the gas
Λ	parameter defined after equation (37)
λ_m	effective thermal conductivity in the porous bed
ρ	density
σ	specific heat ratio
ζ	stretched coordinate in the gas phase region adjacent to the interface.

Subscripts

i, o	inner and outer solutions
w	quantities at the impermeable wall
∞	imposed free boundary conditions.

Superscripts

$+$	solutions in the gas phase region
$-$	solutions in the porous bed
$\wedge$	nondimensional quantities.

ductivity of the solid phase is much higher than that of the gas phase.

Although extensive research work has been devoted to heat transfer in porous media, chemically reactive flows in porous media received little attention until recently. Chen *et al.* [13] studied the premixed combustion in a porous medium and found that radiation heat transfer promotes flame stability and propagation speed. Hsu *et al.* [14] studied a similar problem using detailed chemical kinetics, and the effects of porous material, combustor geometry, and kinetic parameters were discussed. Recently Chao *et al.* [15] analyzed the nonpremixed burning of a condensed fuel in a porous medium with a natural convective oxidizer flow adjacent to the wall and obtained a solution for flame temperature, standoff distance and mass consumption rate. Chemical reacting flows in porous media at low temperatures have also been investigated [16–18].

In the present paper, the problem of a chemically reactive stagnation point flow in a catalytic porous bed will be theoretically investigated. The mathematical formulation of the problem will first be described. The steady reaction characteristics in a thin and a thick porous bed will be subsequently analyzed by a perturbation method. Numerical solutions will be carried out for the steady and transient periods. The effects of different parameters on heat transfer and reaction characteristics in the gas region and the porous bed will also be discussed.

2. FORMULATION

The problem to be analyzed is a laminar, premixed chemically reactive stagnation point flow in a catalytic porous bed of finite thickness H, with the origin of the coordinate system placed at the stagnation point as shown in Fig. 1. The flow is bounded by an impermeable surface at the far side of the catalytic bed. The two-dimensional stagnation point flow can be divided into two regions: a homogeneous gas phase region before the flow enters the porous bed and a two phase, solid–gas region within the bed. Since the system is usually operating at relatively low temperatures comparing to the normal flame temperature, and temperature variations in the whole flow field are not significant, the flow density ρ, gaseous thermal conductivity λ, mass diffusion coefficient D, and gaseous

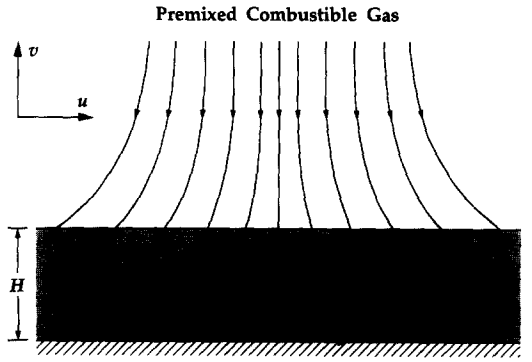

Fig. 1. Schematic defining the problem to be studied.

specific heat at constant pressure c_p can be considered as constants. This allows decoupling of the continuity and momentum equations from the energy and species equations so that only the latter needs to be solved. The reaction rate is assumed to follow a single-reactant, first order, one-step Arrhenius kinetics. Radiation is neglected due to the low flow temperature.

Since the two regions described are controlled by different transport characteristics, the conservation equations need to be formulated separately. In the gas phase region bounded by $H < y < \infty$ (Fig. 1), we have a potential flow so that the solution of the velocity field is $u = kx$ and $v = -ky$ where x and y are the spatial coordinates parallel and normal to the impermeable surface, and u and v the velocity components along x and y directions. The velocity gradient k is the parameter describing the flow strain rate. Due to the high activation energy and low flow temperature in this region, chemical reaction is negligible so that the energy and species conservation equations are

$$\frac{\partial T^+}{\partial t} - ky\frac{\partial T^+}{\partial y} - \frac{\lambda}{\rho c_p}\frac{\partial^2 T^+}{\partial y^2} = 0 \tag{1}$$

$$\frac{\partial Y^+}{\partial t} - ky\frac{\partial Y^+}{\partial y} - D\frac{\partial^2 Y^+}{\partial y^2} = 0 \tag{2}$$

with the boundary conditions

$$y \to \infty: \quad T^+ \to T_\infty \quad Y^+ \to Y_\infty. \tag{3}$$

In the above, t is the time, T the temperature, Y the mass fraction of the controlling species, and the superscript "+" denotes the quantities in the gas phase region, and T_∞ and Y_∞ are prescribed.

In the porous bed, $0 < y < H$, Darcy's law is adopted, so the macroscopic flow field is again a potential flow and the flow velocity is given by $(kx/K, -ky/K)$ where K is the permeability of the porous medium. Multiplying the flow velocity by K, we obtain the Darcy's velocity, which can be applied to the formulation of energy and species conservation equations as

$$\sigma\frac{\partial T^-}{\partial t} - ky\frac{\partial T^-}{\partial y} - \frac{\lambda_m}{\rho c_p}\frac{\partial^2 T^-}{\partial y^2} = \frac{qB}{\rho c_p} Y^- \exp\left(-\frac{E}{R^\circ T^-}\right) \tag{4}$$

$$\frac{\partial Y^-}{\partial t} - ky\frac{\partial Y^-}{\partial y} - D\frac{\partial^2 Y^-}{\partial y^2} = -\frac{B}{\rho} Y^- \exp\left(-\frac{E}{R^\circ T^-}\right) \tag{5}$$

where λ_m is the effective stagnant thermal conductivity in the porous medium, q the heat of combustion per unit mass of the species consumed, E the activation energy, $\sigma = [\varphi c_p + (1-\varphi)c_s]/c_p$ the specific heat ratio, R° the universal gas constant, B the pre-exponential factor representing the collision frequency, φ the porosity of the porous bed, c_s the specific heat of the solid porous material, and the superscript "$-$" denotes quantities in the porous region. Both λ_m and σ are functions of the constitutive characteristics of the fluid and solid. To obtain equation (4), local thermal equilibrium between solid and fluid phases is assumed.

The boundary condition for the energy equation at the impermeable wall (at $y = 0$) depends on the cases specified. It is $T^- = T_w$ for an isothermal wall and $\partial T^-/\partial y = 0$ for an adiabatic wall. For the species equation, there is no net flux and hence $vY^- - D(\partial Y^-/\partial y) = 0$, which can be further reduced to $\partial Y^-/\partial y = 0$ because $v = 0$ at $y = 0$. At the interface between these two regions, $y = H$, the temperature and the species concentration must be continuous. In addition, the flux transported from one region must be transported into the other. Thus the interface conditions are

$$y = H: \quad T^+ = T^-; \quad Y^+ = Y^-,$$

$$\lambda(\partial T^+/\partial y) = \lambda_m(\partial T^-/\partial y); \quad \partial Y^+/\partial y = \partial Y^-/\partial y. \tag{6}$$

The required initial conditions will be specified later. Because the normal flow velocity v and all the boundary conditions are independent of x, the solution is expected to be independent of x so that $\partial/\partial x = 0$ in the conservation equations.

Introducing the nondimensional quantities

$$\hat{T} = \frac{T - T_\infty}{qY_\infty/c_p} \quad \hat{T}_\infty = \frac{c_p T_\infty}{qY_\infty} \quad \hat{Y} = \frac{Y}{Y_\infty}$$

$$\hat{y} = y\Big/\left(\frac{\lambda}{\rho k c_p}\right)^{1/2} \quad \hat{E} = \frac{E/R^\circ}{qY_\infty/c_p} \quad \hat{t} = kt$$

$$\hat{\lambda} = \frac{\lambda_m}{\lambda} \quad Le = \frac{\lambda/c_p}{\rho D} \quad Da = \frac{B}{\rho k}$$

where Le is the Lewis number meaning the ratio of gaseous thermal diffusivity to mass diffusivity, Da the Damköhler number representing the chemical reactivity and $\hat{\lambda}$ the ratio of thermal conductivities, the system is nondimensionalized to

$$\sigma\frac{\partial\hat{T}^-}{\partial\hat{t}}-\hat{v}\frac{\partial\hat{T}^-}{\partial\hat{y}}-\hat{\lambda}\frac{\partial^2\hat{T}^-}{\partial\hat{y}^2}=Da\hat{Y}^-\exp\left(-\frac{\hat{E}}{\hat{T}^-+\hat{T}_\infty}\right) \tag{7}$$

$$\frac{\partial\hat{Y}^-}{\partial\hat{t}}-\hat{v}\frac{\partial\hat{Y}^-}{\partial\hat{y}}-\frac{1}{Le}\frac{\partial^2\hat{Y}^-}{\partial\hat{y}^2}=-Da\hat{Y}^-\exp\left(-\frac{\hat{E}}{\hat{T}^-+\hat{T}_\infty}\right) \tag{8}$$

$$\frac{\partial\hat{T}^+}{\partial\hat{t}}-\hat{v}\frac{\partial\hat{T}^+}{\partial\hat{y}}-\frac{\partial^2\hat{T}^+}{\partial\hat{y}^2}=0 \tag{9}$$

$$\frac{\partial\hat{Y}^+}{\partial\hat{t}}-\hat{v}\frac{\partial\hat{Y}^+}{\partial\hat{y}}-\frac{1}{Le}\frac{\partial^2\hat{Y}^+}{\partial\hat{y}^2}=0 \tag{10}$$

$$\hat{y}=0:\quad \partial\hat{Y}^-/\partial\hat{y}=0$$

$\hat{T}^- = \hat{T}_w$ (isothermal wall) or

$$\partial\hat{T}^-/\partial\hat{y}=0 \text{ (adiabatic wall)} \tag{11}$$

$$\hat{y}=\hat{H}:\quad \hat{T}^+=\hat{T}^-\quad \frac{\partial\hat{T}^+}{\partial\hat{y}}=\hat{\lambda}\frac{\partial\hat{T}^-}{\partial\hat{y}}$$

$$\hat{Y}^+=\hat{Y}^-\quad \frac{\partial\hat{Y}^+}{\partial\hat{y}}=\frac{\partial\hat{Y}^-}{\partial\hat{y}} \tag{12}$$

$$\hat{y}\to\infty:\quad \hat{T}^+\to 0\quad \hat{Y}^+\to 1. \tag{13}$$

The value of $\hat{\lambda}$ can be determined from Cheng [12], which is usually large ($\hat{\lambda}\gg 1$) because the thermal conductivity of solids is larger compared to that of gases.

Due to the catalytic reaction at the surface of catalyst porous material, chemical reaction can occur under low temperature conditions. Thus the function of the catalytic porous bed is to reduce activation energy so that appreciable reaction can occur at a temperature much lower than necessary for conventional combustion processes. Moreover, due to the large thermal inertia of the solid porous material, catalytic reactors can sustain stable reaction for fuel concentrations much below the lean flammability limit in conventional combustion situations [19]. Strong catalytic reaction is considered in this study so that the low activation energy limit, $\hat{E}\ll 1$, is adopted and the Arrhenius term can be linearized to

$$\exp\left(-\frac{\hat{E}}{\hat{T}^-+\hat{T}_\infty}\right)=1-\frac{\hat{E}}{\hat{T}^-+\hat{T}_\infty}+\cdots. \tag{14}$$

The catalytic effect also leads to the distributed reaction throughout the porous bed without a localized vigorous flame.

3. STEADY-STATE ANALYSIS FOR A THIN BED

3.1. *Analysis*

For the steady-state situation, equations (7)–(12) are reduced to

$$\hat{\lambda}\frac{d^2\hat{T}^-}{d\hat{y}^2}+\hat{v}\frac{d\hat{T}^-}{d\hat{y}}=-Da\hat{Y}^-\left(1-\frac{\hat{E}}{\hat{T}^-+\hat{T}_\infty}+\cdots\right) \tag{15}$$

$$\frac{1}{Le}\frac{d^2\hat{Y}^-}{d\hat{y}^2}+\hat{v}\frac{d\hat{Y}^-}{d\hat{y}}=Da\hat{Y}^-\left(1-\frac{\hat{E}}{\hat{T}^-+\hat{T}_\infty}+\cdots\right) \tag{16}$$

$$\frac{d^2\hat{T}^+}{d\hat{y}^2}+\hat{v}\frac{d\hat{T}^+}{d\hat{y}}=0 \tag{17}$$

$$\frac{1}{Le}\frac{d^2\hat{Y}^+}{d\hat{y}^2}+\hat{v}\frac{d\hat{Y}^+}{d\hat{y}}=0 \tag{18}$$

$$\hat{y}=0:\quad d\hat{Y}^-/d\hat{y}=0$$

$\hat{T}^- = \hat{T}_w$ (isothermal wall) or

$$d\hat{T}^-/d\hat{y}=0 \text{ (adiabatic wall)} \tag{19}$$

$$\hat{y}=\hat{H}:\quad \hat{T}^+=\hat{T}^-\quad \frac{d\hat{T}^+}{d\hat{y}}=\hat{\lambda}\frac{d\hat{T}^-}{d\hat{y}}$$

$$\hat{Y}^+=\hat{Y}^-\quad \frac{d\hat{Y}^+}{d\hat{y}}=\frac{d\hat{Y}^-}{d\hat{y}}. \tag{20}$$

Because $\hat{\lambda}$ is large, a small parameter ε can be defined as $\varepsilon=\hat{\lambda}^{-1/2}$ and the solutions of $\hat{T}^\pm$ and $\hat{Y}^\pm$ can be expanded as

$$\hat{T}^\pm=\hat{T}_0^\pm+\varepsilon\hat{T}_1^\pm+\varepsilon^2\hat{T}_2^\pm+\varepsilon^3\hat{T}_3^\pm+O(\varepsilon^4) \tag{21}$$

$$\hat{Y}^\pm=\hat{Y}_0^\pm+\varepsilon\hat{Y}_1^\pm+O(\varepsilon^2). \tag{22}$$

In the gas phase region, substituting equations (21) and (22) into equations (17) and (18) and solving subject to equation (13) yield

$$\hat{T}^+=[a_0^++\varepsilon a_1^++O(\varepsilon^2)]\operatorname{erfc}(\hat{y}) \tag{23}$$

$$\hat{Y}^+=1+[b_0^++\varepsilon b_1^++O(\varepsilon^2)]\operatorname{erfc}[\sqrt{(Le)}\hat{y}] \tag{24}$$

where the complementary error function is defined as

$$\operatorname{erfc}(\chi)=\sqrt{(2/\pi)}\int_\chi^\infty \exp(-\bar{\chi}^2/2)\,d\bar{\chi}.$$

In the porous bed, since the activation energy is considered low, we assume that it is of $O(\varepsilon)$ so that it can be scaled as $\hat{E}=\varepsilon\tilde{E}$. Substituting equations (21) and (22) into equations (15), (16) and (20), we obtain

$$d^2\hat{T}_i^-/d\hat{y}^2=0;\quad i=0,1 \tag{25}$$

$$\frac{d^2\hat{T}_2^-}{d\hat{y}^2}+\hat{v}\frac{d\hat{T}_0^-}{d\hat{y}}=-Da\hat{Y}_0^- \tag{26}$$

$$\frac{d^2\hat{T}_3^-}{d\hat{y}^2}+\hat{v}\frac{d\hat{T}_1^-}{d\hat{y}}=-Da\left(\hat{Y}_1^--\frac{\tilde{E}\hat{Y}_0^-}{\hat{T}_0^-+\hat{T}_\infty}\right) \tag{27}$$

$$\frac{1}{Le}\frac{d^2\hat{Y}_0^-}{d\hat{y}^2}+\hat{y}\frac{d\hat{Y}_0^-}{d\hat{y}}=Da\hat{Y}_0^- \tag{28}$$

$$\frac{1}{Le}\frac{d^2\hat{Y}_1^-}{d\hat{y}^2}+\hat{y}\frac{d\hat{Y}_1^-}{d\hat{y}}=Da\left(\hat{Y}_1^- -\frac{\tilde{E}\hat{Y}_0^-}{\hat{T}_0^-+\hat{T}_\infty}\right) \tag{29}$$

with the interface conditions

$$\hat{y}=\hat{H}:\quad \hat{T}_i^+=\hat{T}_i^- \quad \hat{Y}_i^+=\hat{Y}_i^-$$

$$d\hat{Y}_i^-/d\hat{y}=d\hat{Y}_i^+/d\hat{y};\quad i=0,1 \tag{30a}$$

$$d\hat{T}_0^-/d\hat{y}=d\hat{T}_1^-/d\hat{y}=0 \tag{30b}$$

$$d\hat{T}_2^-/d\hat{y}=d\hat{T}_0^+/d\hat{y}\quad d\hat{T}_3^-/d\hat{y}=d\hat{T}_1^+/d\hat{y}. \tag{30c}$$

Solving equations (25), (28) and (29) subject to equation (19), we obtain

$$\hat{T}^-=\hat{T}_w+[a_0^-+\varepsilon a_1^-+O(\varepsilon^2)]\hat{y}\quad\text{(isothermal wall)} \tag{31a}$$

$$\hat{T}^-=a_0^-+\varepsilon a_1^-+O(\varepsilon^2)\quad\text{(adiabatic wall)} \tag{31b}$$

$$\hat{Y}_0^-=b_0^-F_1(\hat{y}) \tag{32}$$

$$\hat{Y}_1^-=[b_1^-+G_1(\hat{y})]F_1(\hat{y})+\hat{y}G_2(\hat{y})F_2(\hat{y}) \tag{33}$$

where

$$F_1(\hat{y})=1+\sum_{j=1}^{\infty}\left[\prod_{n=0}^{j-1}(Da-2n)\right]\frac{(Le\hat{y}^2)^j}{(2j)!}$$

$$F_2(\hat{y})=1+\sum_{j=1}^{\infty}\left[\prod_{n=1}^{j}(Da+1-2n)\right]\frac{(Le\hat{y}^2)^j}{(2j+1)!}$$

$$G_1(\hat{y})=(LeDa\tilde{E})\int_0^{\hat{y}}\frac{\hat{y}\hat{Y}_0^-F_2/(\hat{T}_0^-+\hat{T}_\infty)}{F_1F_2+\hat{y}(F_1F_2'-F_2F_1')}d\hat{y}$$

$$G_2(\hat{y})=-(LeDa\tilde{E})\int_0^{\hat{y}}\frac{\hat{Y}_0^-F_1/(\hat{T}_0^-+\hat{T}_\infty)}{F_1F_2+\hat{y}(F_1F_2'-F_2F_1')}d\hat{y}$$

and $F_j'=dF_j/d\hat{y}$. In the above, $a_j^{\pm}$ and $b_j^{\pm}$ are the integration constants to be determined.

For the isothermal wall case, we apply equation (30) to equations (23) and (31a) to yield

$$\hat{T}^-=\hat{T}_w+O(\varepsilon^2) \tag{34}$$

$$\hat{T}^+=\hat{T}_w\,\mathrm{erfc}(\hat{y})/\mathrm{erfc}(\hat{H})+O(\varepsilon^2). \tag{35}$$

Next, applying equation (30a) to equations (24), (32) and (33), we obtain

$$\hat{Y}^+=1+\frac{F_1'(\hat{H})+\varepsilon G_2(\hat{H})[F_1F_2+\hat{H}(F_1F_2'-F_2F_1')]_{\hat{y}=\hat{H}}}{[F_1(\hat{H})/\Lambda]+F_1'(\hat{H})}\times\frac{\mathrm{erfc}[\sqrt{(Le)}\hat{y}]}{\mathrm{erfc}[\sqrt{(Le)}\hat{H}]}+O(\varepsilon^2) \tag{36}$$

$$\hat{Y}^-=\frac{1-\varepsilon G_2(\hat{H})[(\hat{H}+\Lambda)F_2(\hat{H})+\hat{H}\Lambda F_2'(\hat{H})]}{F_1(\hat{H})+\Lambda F_1'(\hat{H})}\times F_1(\hat{y})+\varepsilon\{[G_1(\hat{y})-G_1(\hat{H})]F_1(\hat{y})+\hat{y}G_2(\hat{y})F_2(\hat{y})\}+O(\varepsilon^2) \tag{37}$$

where $\Lambda=\sqrt{[\pi/(2Le)]}\,\mathrm{erfc}[\sqrt{(Le)}\hat{H}]\exp(Le\hat{H}^2/2)$.

For the adiabatic wall case, equation (30b) is automatically satisfied and additional conditions are needed. These conditions can be obtained by applying equation (38) to equations (26) and (27), integrating the resulting equations once, and then substituting to equation (30c) to yield

$$\frac{d\hat{T}_0^+}{d\hat{y}}(\hat{H})=-Da\int_0^{\hat{H}}\hat{Y}_0^-\,d\hat{y}$$

$$\frac{d\hat{T}_1^+}{d\hat{y}}(\hat{H})=-Da\int_0^{\hat{H}}\left(\hat{Y}_1^- -\frac{\tilde{E}\hat{Y}_0^-}{\hat{T}_0^-+\hat{T}_\infty}\right)d\hat{y}. \tag{38}$$

Applying equations (30a) and (38) to equations (23) and (31b), $\hat{T}^{\pm}$ can be determined as

$$\hat{T}^-=\sqrt{\left(\frac{\pi}{2}\right)}Da\exp\left(\frac{\hat{H}^2}{2}\right)\mathrm{erfc}\,(\hat{H})\times\int_0^{\hat{H}}\left[\hat{Y}_0^-+\varepsilon\left(\hat{Y}_1^- -\frac{\tilde{E}\hat{Y}_0^-}{\hat{T}_0^-+\hat{T}_\infty}\right)+O(\varepsilon^2)\right]d\hat{y} \tag{39}$$

$$\hat{T}^+=\sqrt{\left(\frac{\pi}{2}\right)}Da\exp\left(\frac{\hat{H}^2}{2}\right)\mathrm{erfc}\,(\hat{y})\times\int_0^{\hat{H}}\left[\hat{Y}_0^-+\varepsilon\left(\hat{Y}_1^- -\frac{\tilde{E}\hat{Y}_0^-}{\hat{T}_0^-+\hat{T}_\infty}\right)+O(\varepsilon^2)\right]d\hat{y}. \tag{40}$$

The solution of $\hat{Y}$ is also given by equations (36) and (37).

3.2. *Results and discussion*

The thermal–chemical characteristics in the flow field depends on the reactants and their concentration for the actual running situations. To demonstrate the salient features of the solution more clearly, we assume that the reactants are supplied at 300 K and the adiabatic flame temperature is 2180 K so that $\hat{T}_\infty=0.1376$. Other values used for computations are $Le=1$, $Da=1$, $\tilde{E}=1$ and $\hat{\lambda}=1/\varepsilon^2=20$ unless otherwise specified. Numerical integration is necessary for the expressions in the integral form, which is carried out by a Gaussian quadrature method.

For the isothermal wall case, we assume the wall temperature to be 700 K and hence $\hat{T}_w=0.3211$. Figure 2(a) shows the profiles of temperature $\hat{T}$ and mass fraction $\hat{Y}$ vs $\hat{y}$ for selected bed thickness $\hat{H}$. In the porous bed, the temperature remains a constant to the second-order approximation because of the high effective thermal conductivity, which can be seen from equation (34). The heat generated through the reaction is completely transferred to the gas phase to preheat the gaseous flow and to the impermeable surface.

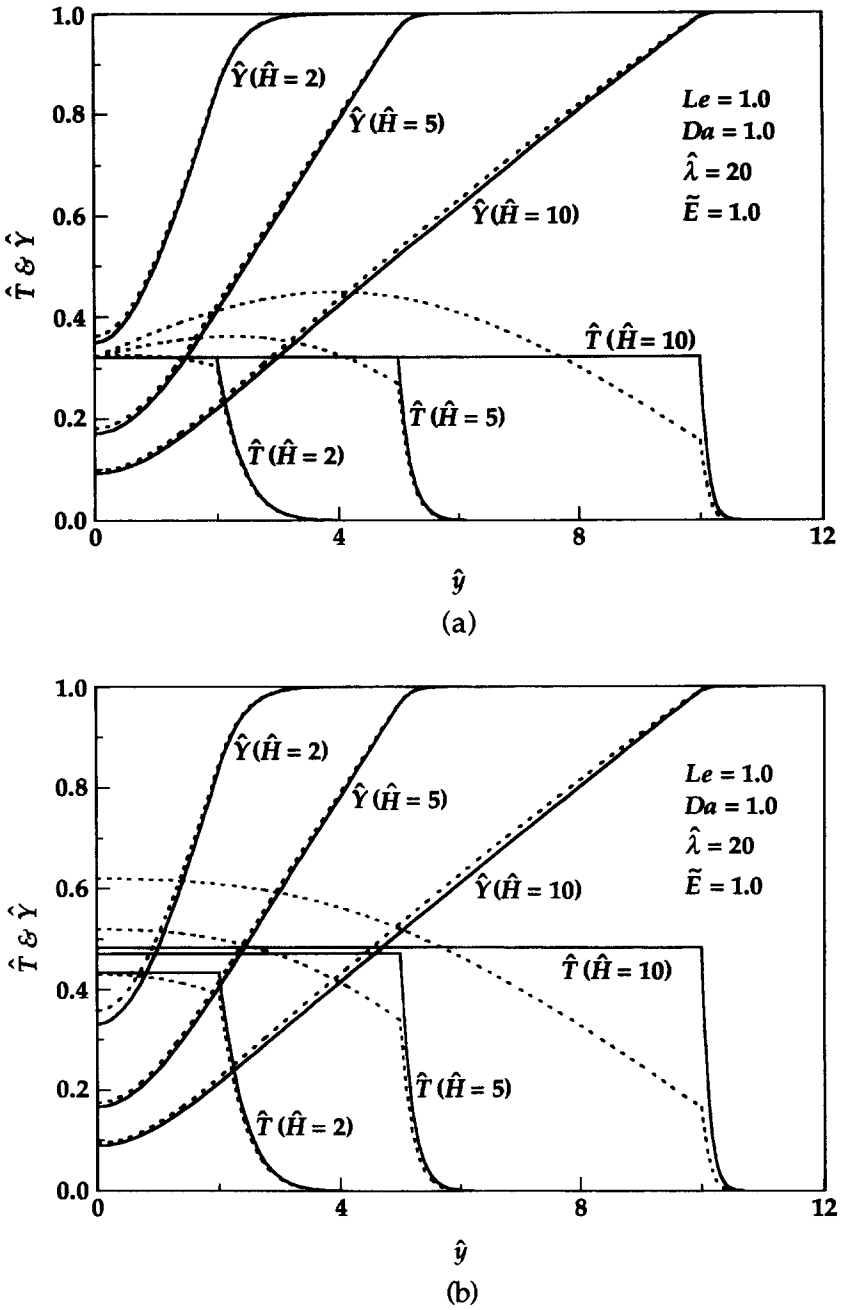

Fig. 2. Variations of temperature $\hat{T}$ and reactant concentration $\hat{Y}$ vs the spatial coordinate $\hat{y}$ for a thin bed with an (a) isothermal wall and (b) adiabatic wall. The broken curves are the numerical solutions.

The gas temperature then increases when approaching the interface. Because of the catalytic reaction, $\hat{Y}$ decreases with decreasing $\hat{y}$ in the porous bed, as expected. The value of $\hat{Y}$ starts decreasing from unity before the flow enters the porous bed due to mass diffusion. The effect of bed thickness on the reactant concentration is also presented in Fig. 2(a). For a thicker bed (larger $\hat{H}$), the resident time is larger so that the conversion from reactants to products is higher, and the reactant concentration is lower.

To assess the accuracy of the perturbation analysis, equations (13) and (15)–(20) are solved numerically using the same parameters by a sixth-order Runge–Kutta method. The results are presented in Fig. 2(a) in dashed curves for comparison. It is shown that the perturbation and numerical solutions for $\hat{Y}$ agree well with each other. The results for the temperature profile, however, are different. When the porous bed is thin, say $\hat{H}=2$, the agreement between these two approaches is satisfactory. By increasing the bed

thickness, the agreement becomes poorer, which means that the perturbation analysis cannot properly describe the heat transfer process when the porous bed is thick. This is due to high flow velocities in the gaseous region and in most of the porous bed except near the wall. As a consequence, convection transport is comparable with diffusion in the energy equation, so that the analysis that neglects the convection effect cannot be applied, and a separate analysis is necessary.

For the adiabatic wall case, there is no heat transfer to the wall and the wall temperature is determinable, and the solution is shown in Fig. 2(b) using the same parameters. The heat and mass transfer characteristics are similar to those for the isothermal wall case, except that there is no temperature gradient at the wall, and the wall temperature depends on the bed thickness. The temperature in the porous bed is higher for a thicker bed because more reactants are converted to products and more heat is generated through the reaction. Similar to the isothermal wall case, the perturbation solution is not applicable when the bed is thick.

The effect of Lewis number on the solutions for the isothermal and adiabatic wall cases is shown in Fig. 3. For gaseous flows, Le is close to unity so the range is selected to be 0.5–1.5. Since Le is the ratio of gaseous thermal diffusivity to mass diffusivity, a lower Le means a higher mass diffusion rate when the thermal diffusion rate is held fixed. Thus for a smaller Le, the reactant concentration is lower in the region relatively far away from the wall because the reactant is diffused into the porous bed at a higher rate. Because the chemical reactivity is fixed, reaction rate depends mainly on the concentration so that more reactant is consumed and more heat is generated. Thus, the temperature is higher for the adiabatic wall case, but remains the same for the isothermal wall case, as shown in Fig. 3 because of the high effective thermal conductivity. Although more reactants are converted to products, all the extra reactants cannot be consumed. The remaining is accumulated in the region near the wall which results in a higher concentration. In the region extremely far away from the surface, the reactant concentration is not affected by Le because the mass transport is convection controlled. The effects of Da and $\tilde{E}$ are qualitatively similar to those for the thick bed case and will be discussed later.

4. STEADY-STATE ANALYSIS FOR A THICK BED

4.1. *Analysis*

From the previous section, we understand that by gradually increasing the bed thickness H or the flow strain rate k till $\hat{H} = O(1/\varepsilon)$, the analysis cannot properly describe the heat transfer process so that a different analysis is necessary. For this thick bed situation, by letting $\hat{H} = 1/(\varepsilon h)$ where h is an $O(1)$ parameter representing the reciprocal of rescaled bed thickness, we can define a new spatial coordinate $z = \hat{y}/\hat{H} = \varepsilon h\hat{y}$. Applying this new coordinate to equations (12), (13) and (15)–(20), the transformed equations are

$$h^2\frac{\mathrm{d}^2\hat{T}^-}{\mathrm{d}z^2} + z\frac{\mathrm{d}\hat{T}^-}{\mathrm{d}z} = -Da\hat{Y}^-\left(1 - \frac{\varepsilon\tilde{E}}{\hat{T}^- + \hat{T}_\infty} + \cdots\right) \tag{41}$$

$$\varepsilon^2\frac{h^2}{Le}\frac{\mathrm{d}^2\hat{Y}^-}{\mathrm{d}z^2} + z\frac{\mathrm{d}\hat{Y}^-}{\mathrm{d}z} = Da\hat{Y}^-\left(1 - \frac{\varepsilon\tilde{E}}{\hat{T}^- + \hat{T}_\infty} + \cdots\right) \tag{42}$$

$$\varepsilon^2 h^2\frac{\mathrm{d}^2\hat{T}^+}{\mathrm{d}z^2} + z\frac{\mathrm{d}\hat{T}^+}{\mathrm{d}z} = 0 \tag{43}$$

$$\varepsilon^2\frac{h^2}{Le}\frac{\mathrm{d}^2\hat{Y}^+}{\mathrm{d}z^2} + z\frac{\mathrm{d}\hat{Y}^+}{\mathrm{d}z} = 0 \tag{44}$$

$z = 0$: $\hat{T}^- = \hat{T}_w$ (isothermal wall) or

$$\mathrm{d}\hat{T}^-/\mathrm{d}z = 0 \text{ (adiabatic wall)} \quad \mathrm{d}\hat{Y}^-/\mathrm{d}z = 0 \tag{45}$$

$$z \to \infty: \quad \hat{T}^+ \to 0 \quad \hat{Y}^+ \to 1 \tag{46}$$

$$z = 1: \quad \hat{T}^+ = \hat{T}^- \quad \varepsilon^2\frac{\mathrm{d}\hat{T}^+}{\mathrm{d}z} = \frac{\mathrm{d}\hat{T}^-}{\mathrm{d}z}$$

$$\hat{Y}^+ = \hat{Y}^- \quad \frac{\mathrm{d}\hat{Y}^+}{\mathrm{d}z} = \frac{\mathrm{d}\hat{Y}^-}{\mathrm{d}z}. \tag{47}$$

In the gas phase region, $z > 1$, the transport process is convection controlled. Substituting equations (21) and (22) into equations (43) and (44) and solving subject to equation (46) yield $\hat{T}_o^+ \equiv 0$ and $\hat{Y}_o^+ \equiv 1$. Since the interface conditions in equation (47) cannot be satisfied, there is a thin layer adjacent to the interface in which the characteristics of heat and mass transport is different. A subscript "o" is used to denote solutions in the outer region away from the interface. In the thin inner layer, diffusion and convection transports are comparable so the coordinate need be stretched as $\zeta = (z-1)/(\varepsilon h)^2$. Applying ζ to equations (43) and (44), expanding and solving the resulting equations yield

$$\hat{T}_i^+ = [a_{i,0}^+ + \varepsilon a_{i,1}^+ + O(\varepsilon^2)]\,\mathrm{e}^{-\zeta} \tag{48}$$

$$\hat{Y}_i^+ = 1 + [b_{i,0}^+ + \varepsilon b_{i,1}^+ + O(\varepsilon^2)]\,\mathrm{e}^{-Le\zeta} \tag{49}$$

where $a_{i,j}^+$ and $b_{i,j}^+$ are integration constants to be determined, and the subscript "i" denotes the inner solutions. The matching conditions $\hat{T}_i^+(\zeta \to \infty) \to 0$ and $\hat{Y}_i^+(\zeta \to \infty) \to 1$ have been used in obtaining equations (48) and (49). At the interface, $\zeta = 0$, applying equations (48) and (49) into equation (47) yields $b_{i,0}^+ = b_{i,1}^+ = 0$ so that $\hat{Y}_i^+ = 1 + O(\varepsilon^2)$, and the interface conditions become

$$z = 1: \quad \hat{T}^- = -h^2(\mathrm{d}\hat{T}^-/\mathrm{d}z) = a_{i,0}^+ + \varepsilon a_{i,1}^+ + O(\varepsilon^2);$$

$$\hat{Y}^- = 1 + O(\varepsilon^2). \tag{50}$$

In the porous bed, expanding equation (42) and

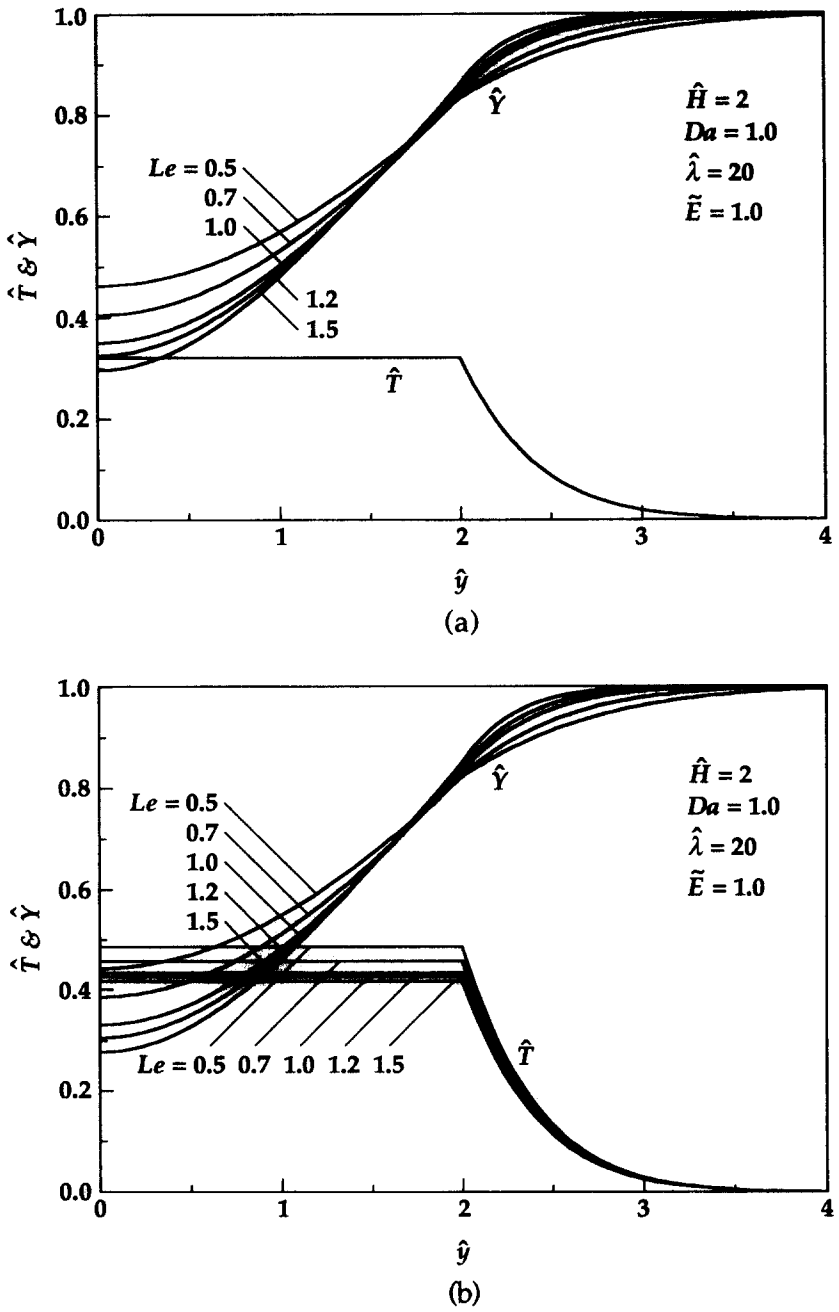

Fig. 3. Temperature $\hat{T}$ and reactant concentration $\hat{Y}$ in response to variations of the Lewis number Le, for a thin bed ($\hat{H} = 2$) with an (a) isothermal wall and (b) adiabatic wall.

solving the resulting equations subject to equation (50) give

$$\hat{Y}_o^- = z^{Da}\left[1+\varepsilon Da\tilde{E}\int_z^1 \frac{dz}{z(\hat{T}_{o,0}^- + \hat{T}_\infty)} + O(\varepsilon^2)\right] \tag{51}$$

which depends on $\hat{T}_{o,0}^-$. Similar to the gas phase analysis, the boundary condition at $z = 0$ cannot be satisfied so that there is another thin boundary layer near the wall. The subscript "o" is then used to denote the outer solutions away from the impermeable wall ($z = 0$). Next expanding equation (41) following equation (21), and solving the two leading order equations subject to equation (50) give

$$\hat{T}_{o,0}^- = a_{1,0}^+ + [(a_{1,0}^+/h^2)+\gamma] \times \int_z^1 \exp[(1-z^2)/(2h^2)]\,dz + \Gamma(z) \tag{52}$$

$$\hat{T}_{o,1}^{-} = a_{i,1}^{+} + [(a_{i,1}^{+}/h^2) + \phi] \times \int_z^1 \exp[(1-z^2)/(2h^2)]\,dz + \Phi(z) \quad (53)$$

where

$$\Gamma(z) = Da \sum_{j=1}^{\infty} \left\{ (-1)^j (z^{Da+2j} - 1) \Big/ \left[h^{2j} (Da+2j) \prod_{n=1}^{j} (Da+2n-1) \right] \right\}$$

$$\Phi(z) = \frac{1}{h^2} \int_z^1 \exp\left(\frac{-z^2}{2h^2}\right) \left[\int_0^z z \frac{d\hat{Y}_{o,1}^{-}}{dz} \exp\left(\frac{z^2}{2h^2}\right) dz \right] dz$$

$$\gamma = \left(\frac{d\Gamma}{dz}\right)_{z=1} = Da \sum_{j=1}^{\infty} \left\{ (-1)^j \Big/ \left[h^{2j} \prod_{n=1}^{j} (Da+2n-1) \right] \right\}$$

$$\phi = \left(\frac{d\Phi}{dz}\right)_{z=1} = -\frac{1}{h^2} \int_0^1 z \frac{d\hat{Y}_{o,1}^{-}}{dz} \exp\left(\frac{z^2-1}{2h^2}\right) dz.$$

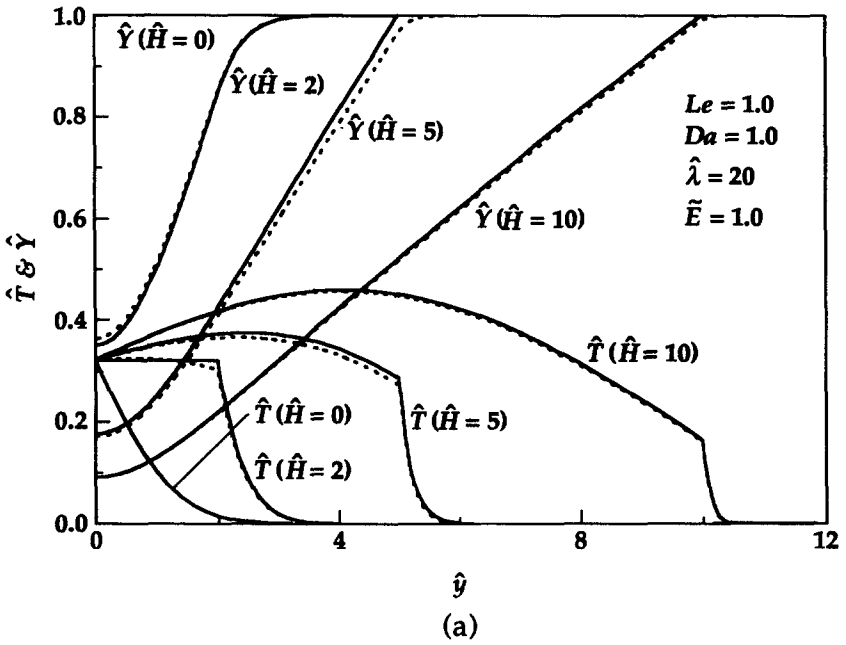

(a)

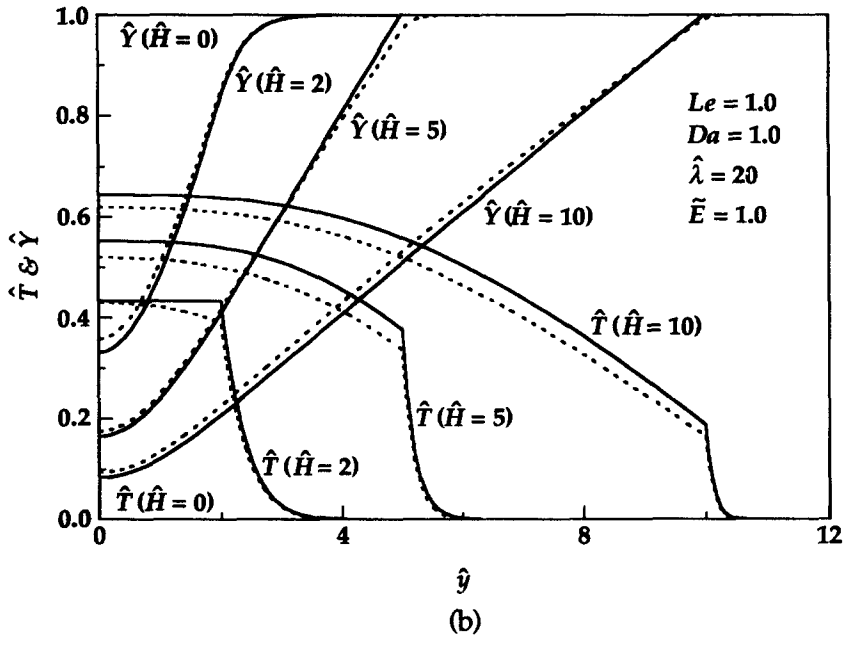

(b)

Fig. 4. Variations of temperature $\hat{T}$ and reactant concentration $\hat{Y}$ vs the spatial coordinate $\hat{y}$ for a thick bed with an (a) isothermal wall and (b) adiabatic wall. The broken curves are the numerical solutions.

In the thin inner region adjacent to the wall, a stretched coordinate $\hat{y} = z/\varepsilon h$ is defined. Applying this coordinate to equations (41), (42) and (45), we recover equations (15), (16) and (19) so that the solution for the thin layer model is applicable in this region. This is expected because the normal flow velocity is relatively low near the wall as in the thin wall case. Thus, by defining

$$\hat{Y}_i^- = (\varepsilon h)^{Da}[\hat{Y}_{i,0}^- + \varepsilon \hat{Y}_{i,1}^- + O(\varepsilon^2)] \quad (54)$$

to properly account for the ordering, the solution can be obtained from equations (32) and (33) as

$$\hat{Y}_i^- = (\varepsilon h)^{Da}\{\langle b_{i,0}^- + \varepsilon[b_{i,1}^- + G_{i,1}(\hat{y})]\rangle F_1(\hat{y}) + \varepsilon \hat{y} G_{i,2}(\hat{y}) F_2(\hat{y}) + O(\varepsilon^2)\} \quad (55)$$

where $b_{i,j}^-$ are integration constants to be determined, and the subscript "i" denotes solutions in the inner region. In the above $G_{i,j}(\hat{y})$ are the $G_j(\hat{y})$ after equation (33) with $\hat{T}_0^-$ and $\hat{Y}_0^-$ replaced by $\hat{T}_{i,0}^-$ and $\hat{Y}_{i,0}^-$.

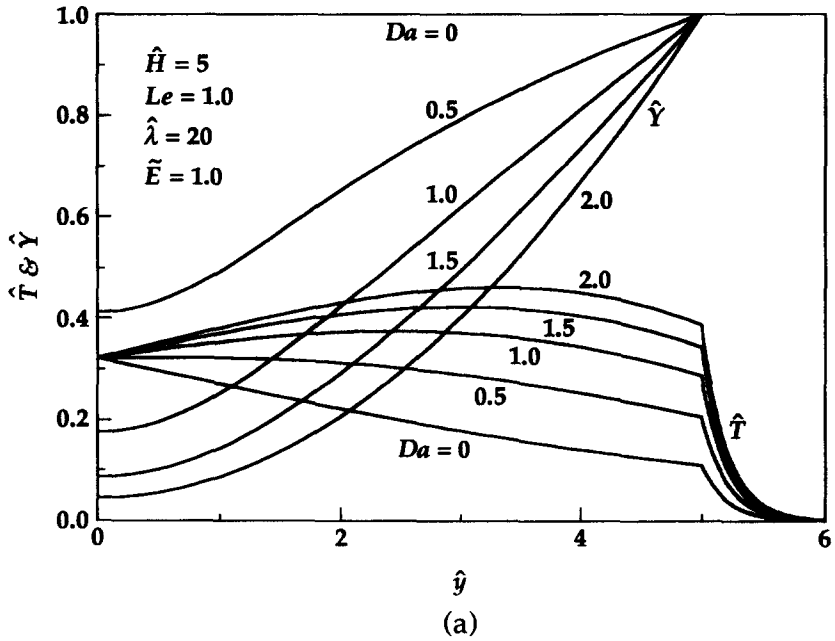

Fig. 5. Temperature $\hat{T}$ and reactant concentration $\hat{Y}$ in response to variations of the Damköhler number Da, for a thick bed with an (a) isothermal wall and (b) adiabatic wall.

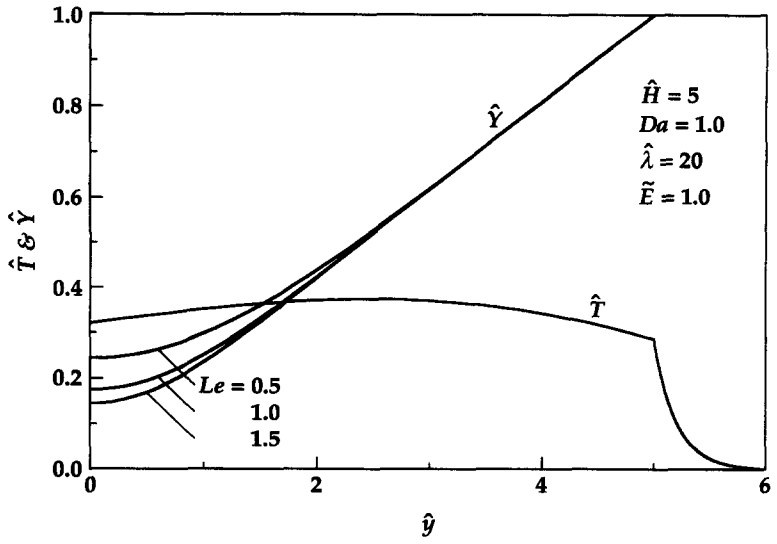

Fig. 6. Temperature $\hat{T}$ and reactant concentration $\hat{Y}$ in response to variations of the Lewis number Le, for a thick bed with an isothermal wall.

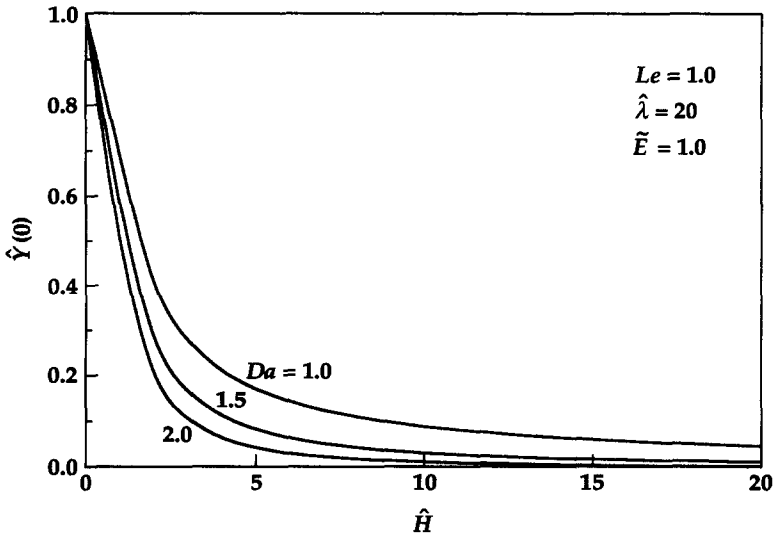

Fig. 7. Reactant concentration at the wall $\hat{Y}(0)$ vs the bed thickness $\hat{H}$, for specified Damköhler number Da, for a thick bed with an isothermal wall.

Matching between the inner and outer solutions yields the matching condition

$$\hat{Y}_i^-(\hat{y}\to\infty) = (\varepsilon h\hat{y})^{Da} \times\left[1+\varepsilon Da\tilde{E}\int_0^1 \frac{dz}{z(\hat{T}_{o,0}^- + \hat{T}_\infty)} + O(\varepsilon^2)\right] \quad (56)$$

$$\hat{T}_i^-(\hat{y}\to\infty) = (a_{i,0}^+ + \varepsilon a_{i,1}^+) + \{[(a_{i,0}^+ + \varepsilon a_{i,1}^+)/h^2] + \gamma + \varepsilon\phi\}\int_0^1 \exp[(1-z^2)/(2h^2)]\,dz + [\Gamma(0) + \varepsilon\Phi(0)] - \varepsilon h\hat{y}[(a_{i,0}^+/h^2) + \gamma] \times \exp[1/(2h^2)] + O(\varepsilon^2). \quad (57)$$

Applying equation (56) to equation (55), we obtain $b_{i,0}^- = (\hat{y}^{Da}/F_1)_{\hat{y}\to\infty}$ and

$$b_{i,1}^- = b_{i,0}^-\left[Da\tilde{E}\int_0^1 \frac{dz/z}{\hat{T}_{o,0}^- + \hat{T}_\infty} - (\hat{y}^{1-Da}G_{i,2}F_2)_{\hat{y}\to\infty}\right] - G_{i,1}(\hat{y}\to\infty). \quad (58)$$

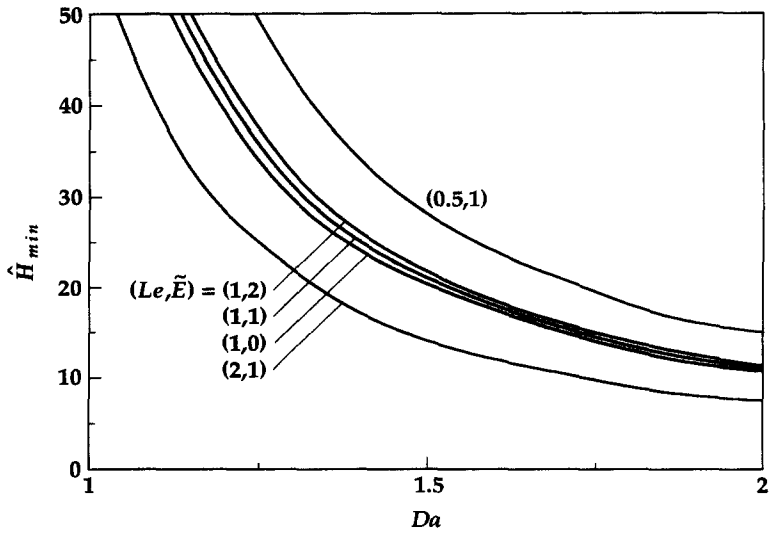

Fig. 8. The minimum bed thickness $\hat{H}_{\min}$, to reach 99% conversion as a function of the Damköhler number Da, Lewis number Le, and activation energy $\tilde{E}$ for the isothermal wall case.

The composite solution in the porous bed can be obtained by adding the outer and inner solutions, then subtracting the solution in their common region to yield

$$\hat{Y}_i^- = \left(\frac{z}{\hat{y}}\right)^{Da}\left\{b_{i,0}^- F_1 + \varepsilon\left[(b_{i,1}^- + G_{i,1})F_1 + \hat{y}G_{i,2}F_2 - Da\tilde{E}\hat{y}^{Da}\int_0^z \frac{dz/z}{\hat{T}_{o,0}^- + \hat{T}_\infty}\right] + O(\varepsilon^2)\right\}. \quad (59)$$

The solution of temperature needs to be further divided to two cases depending on the wall condition. For the isothermal wall case, the solution is given by equation (31a) as

$$\hat{T}_i^- = \hat{T}_w + [a_{i,0}^- + \varepsilon a_{i,1}^- + O(\varepsilon^2)]\hat{y}. \quad (60)$$

Applying the matching condition of equation (57) yields $a_{i,0}^- = 0$

$$a_{i,0}^+ = h^2\left\{\hat{T}_w - \gamma\int_0^1 \exp[(1-z^2)/(2h^2)]\,dz - \Gamma(0)\right\}\Big/\alpha \quad (61)$$

$$a_{i,1}^- = -h\exp[1/(2h^2)][\hat{T}_w - \Gamma(0) + h^2\gamma]/\alpha \quad (62)$$

$$a_{i,1}^+ = -h^2\left\{\phi\int_0^1 \exp[(1-z^2)/(2h^2)]\,dz + \Phi(0)\right\}\Big/\alpha \quad (63)$$

where

$$\alpha = h^2 + \int_0^1 \exp[(1-z^2)/(2h^2)]\,dz.$$

The composite solution in the porous bed can then be determined as

$$\hat{T}^- = \hat{T}_w - \alpha^{-1}[\hat{T}_w - \Gamma(0) - \varepsilon\Phi(0) + h^2(\gamma + \varepsilon\phi)] \times \int_0^z \exp[(1-z^2)/(2h^2)]\,dz + [\Gamma(z) - \Gamma(0)] + \varepsilon[\Phi(z) - \Phi(0)] + O(\varepsilon^2). \quad (64)$$

Moreover, the solution in the gas phase becomes

$$\hat{T}^+ = \frac{h^2}{\alpha}\left[\hat{T}_w - (\gamma + \varepsilon\phi)\int_0^1 \exp\left(\frac{1-z^2}{2h^2}\right)dz - \Gamma(0) - \varepsilon\Phi(0)\right]e^{-\zeta} + O(\varepsilon^2). \quad (65)$$

For the adiabatic wall case, the solution is given by equation (31b) as

$$\hat{T}_i^- = a_{i,0}^- + \varepsilon a_{i,1}^- + O(\varepsilon^2). \quad (66)$$

Applying equation (57) yields $a_{i,0}^+ = a_{i,0}^- - \Gamma(0) = -h^2\gamma$ and $a_{i,1}^+ = a_{i,1}^- - \Phi(0) = -h^2\phi$, so that the composite solution in the porous bed is

$$\hat{T}^- = \Gamma(z) + \varepsilon\Phi(z) - h^2(\gamma + \varepsilon\phi) + O(\varepsilon^2) \quad (67)$$

while the solution in the gas phase becomes

$$\hat{T}^+ = -h^2[\gamma + \varepsilon\phi + O(\varepsilon^2)]\,e^{-\zeta}. \quad (68)$$

4.2. *Results and discussion*

Computations were carried out using the same parameters specified in Section 3. Figure 4(a) shows the temperature and concentration profiles for selected values of the bed thickness $\hat{H}$ for the isothermal wall case. In the limit $\hat{H} = 0$, there is no porous bed and no chemical reaction so that the reactant concentration is a constant. The solution for $\hat{H} = 2$ is extracted from Fig. 2(a) for comparison. Similar to the thin layer

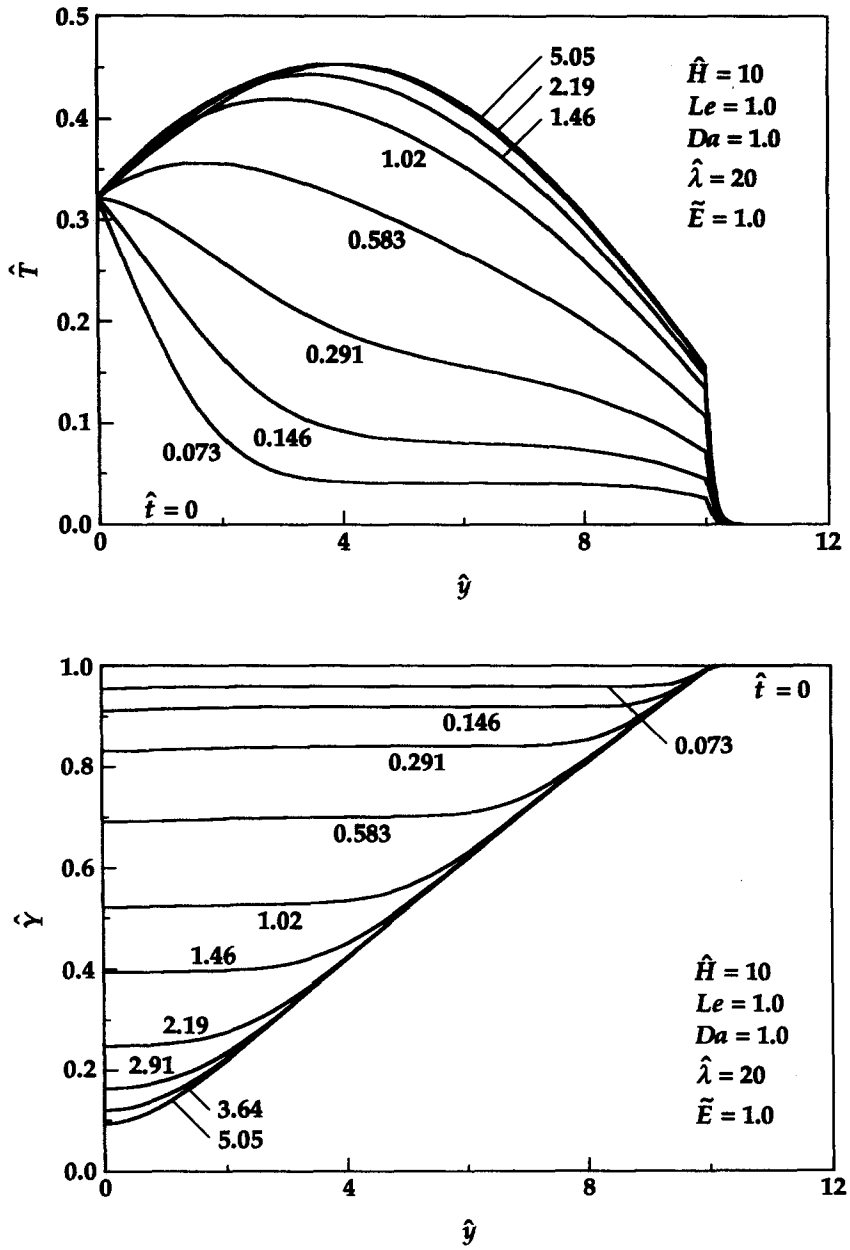

Fig. 9. Evolution of temperature $\hat{T}$ and reactant concentration $\hat{Y}$ with time for the isothermal wall case with $\hat{H} = 10$.

case, $\hat{Y}$ decreases with decreasing $\hat{y}$ in the porous bed. For a thicker bed, the reactant concentration in the porous bed is lower because the resident time is larger so that more reactants are consumed. The concentration remains unchanged in the gas phase since the flow is convection dominated.

There exists a maximum temperature in the porous bed because of the high residence time, which yields a high conversion of reactants and a high heat generation through reaction. Part of the heat generated is accumulated in the bed although the effective thermal conductivity is high. However, it should be mentioned that this phenomenon is not observed when the reaction rate is low. The maximum temperature is higher for a thicker bed because of a higher heat generation. In the gas phase, the temperature gradient is high near the porous bed also because of the strong convection. The corresponding plot for the adiabatic wall case is shown in Fig. 4(b), in which the results are qualitatively similar to the isothermal wall case except that the maximum temperature occurs at the impermeable wall because there is no heat transfer there. To assess the accuracy of the perturbation analysis for a thick bed, equations (41)–(47) were solved numerically by a sixth-order Runge–Kutta method and the results are also presented in Fig. 4. It is shown that agreement

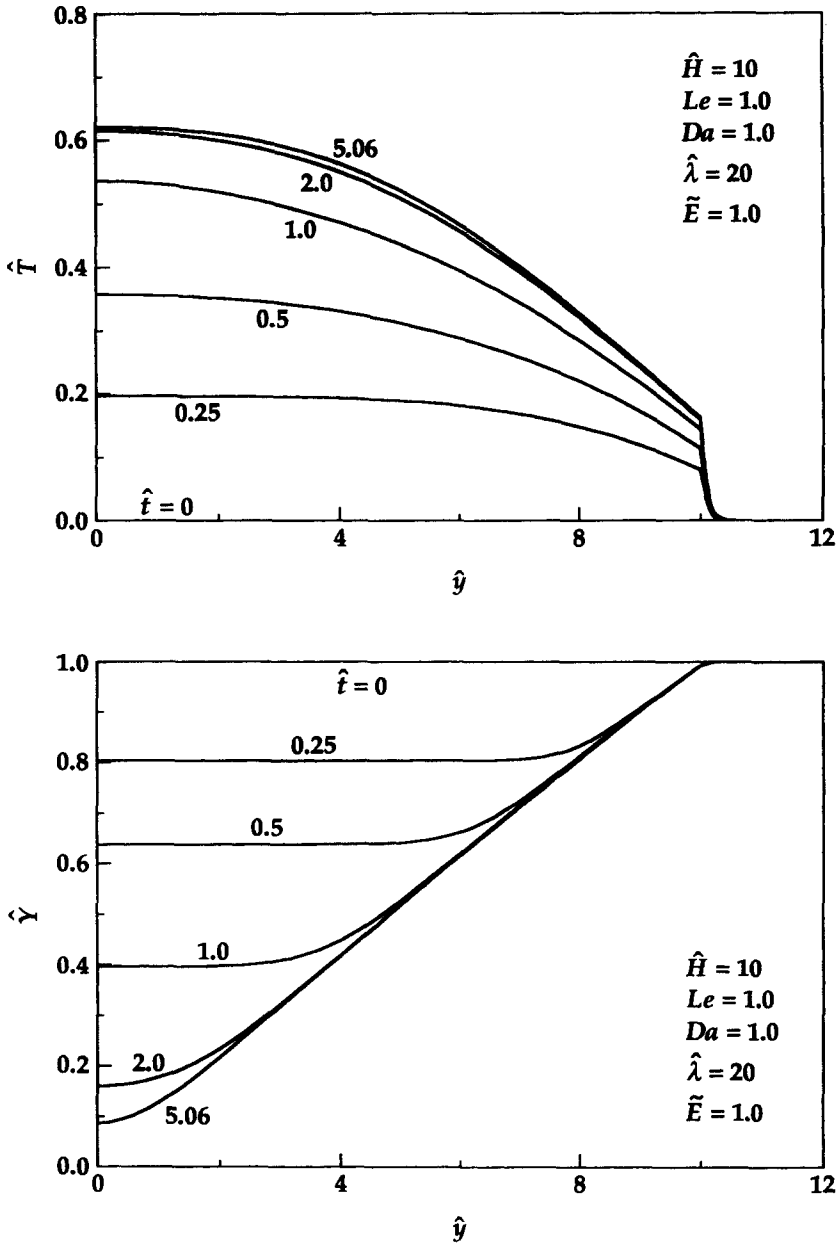

Fig. 10. Evolution of temperature $\hat{T}$ and reactant concentration $\hat{Y}$ with time for the adiabatic wall case with $\hat{H} = 10$.

between the perturbation and numerical solutions is good so that the perturbation analysis properly describes the characteristics of the system.

The effect of the chemical reactivity, expressed by the Damköhler number Da, on the solution is shown in Fig. 5, with the chemically inert limit given by $Da = 0$ and $\hat{Y} = 1$. It is seen that for a higher chemical reaction rate (a larger Da), more reactants are converted to products so the reactant concentration is lower and the temperature is higher. For the isothermal wall case, when Da is small, the heat generated is not sufficient to overcome the outward heat transfer so that there is no local temperature maximum as discussed earlier. Heat is transferred into the system from the impermeable wall for this situation. When Da is sufficiently large (i.e. chemical reaction being sufficiently strong), a maximum temperature appears in the porous bed.

Because low activation energy is considered in this study, $\tilde{E}$ has only weak effects on the solution. Since the activation energy is the energy barrier for the chemical reaction to occur, the reaction is stronger for a smaller $\tilde{E}$ so that the reactant concentration is lower and the temperature is higher. Thus the effect of $\tilde{E}$ is qualitatively similar to Fig. 5 with increasing $\tilde{E}$ equivalent to decreasing Da. Moreover, because the

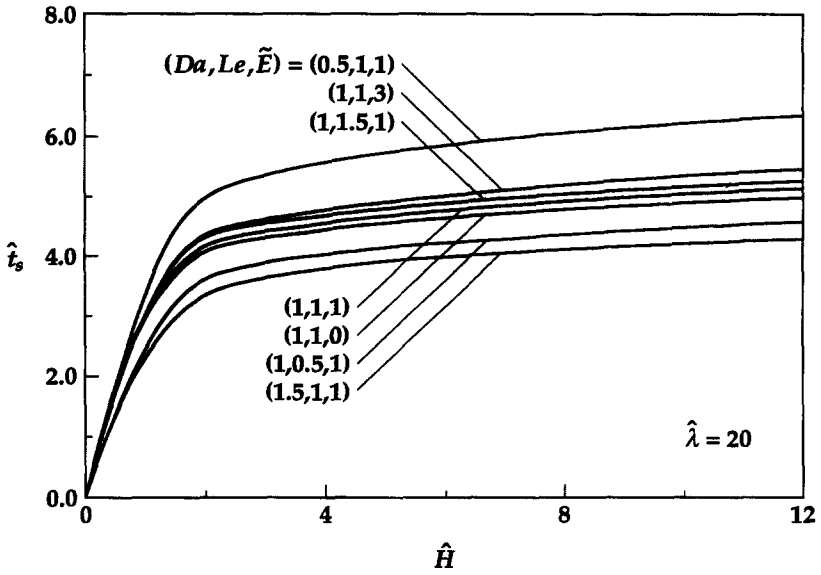

Fig. 11. The transient period $\hat{t}_s$ vs the bed thickness $\hat{H}$, for selected values of the Damköhler number Da, Lewis number Le, and activation energy $\tilde{E}$.

effect of activation energy is linearized, ignition is not possible, which is realistic for catalytic converters.

The effect of the Lewis number for the isothermal wall case is presented in Fig. 6. Because the mass transport is convection-reaction controlled in most of the porous bed, the diffusion transport is significant only in the thin inner region near the wall, in which it is comparable with the convection transport. Thus, the Lewis number effect on the reactant concentration $\hat{Y}$ is weak and needs to be considered only in the thin region near the wall, for which $\hat{Y}$ is higher for smaller Le as observed in Fig. 3(a). Lewis number has only negligibly small effect on the flow temperature because in the inner region where mass diffusion is important, energy transport is controlled by conduction only. The situation for the adiabatic wall case is qualitatively similar and will not be presented.

One of the major objectives of this study is to investigate the minimum porous bed thickness, $\hat{H}_{min}$, for which complete reaction is attained. To obtain this information, we first plot the reactant concentration at the wall, $\hat{Y}(0)$, vs the bed thickness, $\hat{H}$, for selected values of Da. This quantity represents the conversion rate, and is important in the determination of bed thickness for catalytic converters. The results are presented in Fig. 7 for the isothermal wall case, which shows that $\hat{Y}(0)$ decreases with increasing $\hat{H}$ and Da, which is expected from our earlier discussion. The results for the adiabatic wall case are qualitatively identical and quantitatively close to Fig. 7, and will not be presented. The correction of Le and $\tilde{E}$ can be included following our earlier discussion if interested. Since $\hat{Y}(0) \to 0$ only when $\hat{H} \to \infty$, the value of $\hat{H}_{min}$ cannot be obtained. However, if 99% conversion is adopted as complete reaction, $\hat{H}_{min}$ can be plotted vs Da for specified values of Le and $\tilde{E}$ as shown in Fig. 8, which shows that the bed size required to reach complete reaction is thinner for higher Da, lower Le, and lower $\tilde{E}$, as expected following our earlier discussion. Since quantitative difference between the isothermal and adiabatic wall cases are indistinguishably small, Fig. 8 is applicable for both of the cases.

The effect of the flow strain rate k appears in the characteristic length scale used in the non-dimensionalization. By increasing k, the characteristic length scale is reduced so the porous bed behaves like a thicker bed. This is reasonable because the flow velocity is higher and hence the convection transport is stronger. However, the Damköhler number is decreased because the resident time for the chemical reaction to occur is reduced. Therefore, the effect of k is the same as $\hat{H}$ with a lower Da so that a separate discussion is not necessary.

5. TRANSIENT ANALYSIS

During the initial period after the reactive fluid starts passing through the porous bed, a large amount of reactant leaves the bed without being converted to the products because the catalytic porous bed does not operate at its designated condition, so that steady analyses cannot be applied. To complete our study, the flow behavior in the initial transient period is also investigated.

The conservation equations and boundary conditions for the transient study are presented in equations (7)–(13). The initial conditions required to solve the system are obtained by considering the flow to be chemically inert initially, i.e.

$$\hat{t} = 0, \hat{y} > 0: \quad \hat{T} = 0 \quad \hat{Y} = 1. \tag{69}$$

The flow velocity is not affected by the transient behavior because constant density is assumed.

Because analytical solution does not exist for the transient problem, a numerical approach using a finite difference method with forward difference in time and central difference in space is performed. The bed thickness $\hat{H} = 10$ is used to present the result more clearly. Steady state is considered reached when the change of temperature and concentration in a time step is less than 10^{-7}. The solutions of $\hat{T}$ and $\hat{Y}$ as functions of $\hat{y}$ and $\hat{t}$ for the isothermal wall case are shown in Fig. 9. At $\hat{t} = 0$, there is no chemical reaction and the solution is given by equation (69). By continuously increasing $\hat{t}$, the reactant concentration decreases while the temperature increases due to the reaction. Steady state is reached when $\hat{t} \approx 5.05$ for this case. The corresponding solutions for the adiabatic wall are presented in Fig. 10. Similar evolution is observed with the steady state reached at $\hat{t} = 5.06$.

The time required to reach steady state, or the transient period, $\hat{t}_s$, is plotted in Fig. 11 vs the bed thickness $\hat{H}$ for some values of Da, Le and $\tilde{E}$. It is shown that for fixed kinetic and transport parameters, $\hat{t}_s$ is larger for a thicker bed because a larger time is needed to reach a higher conversion rate. For thick beds, the increase of $\hat{t}_s$ with $\hat{H}$ is gradual since the transport is basically convection-reaction controlled. Moreover, $\hat{t}_s$ is smaller with increasing Da and decreasing $\tilde{E}$ because the reaction rate is higher, and decreasing Le because $\hat{Y}(0)$ is higher. Because the difference of $\hat{t}_s$ for the two cases is indistinguishably small, Fig. 11 is applicable to both of them.

6. CONCLUDING REMARKS

In this study, the gaseous flow of chemically reactive premixtures within a catalytic porous bed is theoretically investigated to model the operation of catalytic converters. A laminar stagnation-point flow is adopted to best describe the flow field in the converter. Both the steady-state and initial transient operation situations are analyzed for both the isothermal and adiabatic wall conditions.

For the steady-state situation, reactant concentration and temperature distributions are solved analytically and then compared with numerical solutions. Because the heat and mass transport characteristics are different for thin and thick bed cases, separate analyses are performed. For a thick bed, a multiple layer asymptotic analysis is necessary. Results show that in the porous bed, the temperature is higher and the reactant concentration is lower for a thicker bed, higher chemical reactivity (higher Damköhler number Da), lower activation energy, or lower mass diffusion rate (higher Lewis number Le), because of the higher conversion from reactants to products. The minimum bed thickness required to reach 99% conversion is also obtained vs the above parameters. The analytical solutions agree well with numerical integration of the governing equations.

Because of analytical difficulties, the initial transient period is numerically studied using finite difference methods. The evolution of temperature and reactant concentration with time are obtained, which gives the time required to reach steady state.

The physical parameters for the porous bed such as the pre-exponential factor B, activation energy E, porosity ϕ, and the effective thermal conductivity λ_m depend on the catalytic material selected and can be specified only through experiments. The gas properties are relatively well known, but the exact specification depends on the components of the gaseous mixture.

REFERENCES

1. B. S. Gottfried, Combustion of crude oil in a porous medium, *Combust. Flame* **12,** 5–13 (1968).
2. S. B. Sathe, M. R. Kulkarni, R. E. Peck and T. W. Tong, An experimental and theoretical study of porous radiant burner performance, *Proceedings of the Twenty-Third International Symposium on Combustion*, pp. 1011–1018 (1991).
3. J. McDermott, Catalytic conversion of automobile exhaust, *Pollution Control Review* 2. Noyes Data Corporation, Park Ridge, NJ (1971).
4. A. M. Klimov, Laminar flame in a turbulent flow, *Zh. Prickl. i Tekhn. Fiz.* **3,** 49 (1963).
5. J. D. Buckmaster, The quenching of a deflagration wave held in front of a bluff body, *Proceedings of the Seventeenth International Symposium on Combustion*, pp. 835–842 (1979).
6. B. H. Chao and C. K. Law, Asymptotic theory of flame extinction with surface reaction, *Combust. Flame* **92,** 1–24 (1993).
7. P. A. Libby and F. A. Williams, Structure of laminar flamelets in premixed turbulent flames, *Combust. Flame* **44,** 287–303 (1982).
8. J. Sato and H. Tsuji, Extinction of premixed flames in a stagnation flow considering general Lewis number, *Combust. Sci. Technol.* **33,** 193–205 (1983).
9. C. K. Law and G. I. Sivashinsky, Catalytic extension of extinction limits of stretched premixed flames, *Combust. Sci. Technol.* **29,** 277–286 (1982).
10. V. Giovangigli and S. Candel, Extinction limits of premixed catalyzed flames in stagnation point flows, *Combust. Sci. Technol.* **48,** 1–30 (1986).
11. P. Cheng, Geothermal heat transfer. In *Handbook of Heat Transfer Applications* (Edited by W. Rohsenow, J. P. Hartnett and E. N. Ganic), Chap. 11, pp. 1–54. McGraw-Hill, New York (1985).
12. P. Cheng, Heat conduction in a packed bed with wall effects, *Int. Commun. Heat Mass Transfer* **13,** 11–21 (1986).
13. Y. K. Chen, P. F. Hsu, I. G. Lim, Z. H. Lu, R. D. Matthews, J. R. Howell and S. P. Nichols, Experimental and theoretical investigation of combustion within porous inert media, Poster Paper P22-207, Twenty-Second International Symposium on Combustion (1988).
14. P. F. Hsu, J. R. Howell and R. D. Matthews, A numerical investigation on premixed combustion within porous inert media, Poster Paper, ASME/JSME meeting, Las Vegas, NV (1991).
15. B. H. Chao, P. Cheng and T. Le, Free-convective diffusion flame sheet in porous media, *Combust. Sci. Technol.* **99,** 221–234 (1994).

16. W. Kordylewski and Z. Krajewski, Convective on thermal ignition in porous media, *Chem. Engng Sci.* **39,** 610–612 (1984).
17. H. Viljoen and H. Hlavacek, Chemically driven convection in a porous medium, *A.I.Ch.E. Jl* **33,** 1344–1350 (1987).
18. M. S. Malashetty, P. Cheng and B. H. Chao, Convective instability in a horizontal porous layer saturated with a chemically reacting fluid, *Int. J. Heat Mass Transfer* **37,** 2901–2908 (1994).
19. R. Prasad and L. A. Kennedy, Catalytic combustion—A review, *Catal. Rev.* **26,** 1–58 (1982).